6. Leskinen-Kallio S, Någren K, Lehikoinen P, Ruotsalainen U, Teräs M, Joensuu H. Carbon-11-methionine and PET is an effective method to image head and neck cancer. *J Nucl Med* 1992;33:691–695.
7. Van Venrooij WJ, Kuijper-Lenstra AH, Kramer MF. Inter-relationship between amino acid pools and protein synthesis in the rat submandibular gland. *Biochem Biophys Acta* 1973;312:392–398.
8. Bustamante JC, Mann GE, Yudilevich DL. Specificity of neutral amino acid uptake at the basolateral side of the epithelium in the cat salivary gland in situ. *J Physiol* 1981;313:65–79.
9. Kereyer G, Rossignol B. Effects of carbacol on extracellular Na-dependent uptake in the parotid gland. *Am J Physiol* 1980;239:G183–G189.
10. Takuma T, Baum BJ. Na^+-dependent transport of alfa-aminoisobutyrate in isolated basolateral membrane vesicles from rat parotid glands. *Biochem Biophys Acta* 1985;812:453–459.
11. Boyd CAR, Yudilevich DL. Blood-tissue movement of amino acids in various organs: the basolateral membrane and its importance in the polarity of transepithelial transport. In: Yudilevich DL, Boyd CAR, eds. *Amino acid transport in animal cells*. Manchester UK: Manchester University Press; 1987:120–156.
12. Betz AL, Goldstein GW. The polarity of the blood-brain barrier: neutral amino acid transport into isolated brain capillaries. *Science* 1978;202:225–226.
13. Nuutila P, Koivisto VA, Knuuti J, et al. The glucose-free fatty acid cycle operates in human heart and skeletal muscle in vivo. *J Clin Invest* 1992;89:1767–1744.
14. DeFronzo RA, Tobin JD, Andres R. The glucose clamp technique: a method for quantifying insulin secretion and resistance. *Am J Physiol* 1979;237:E214–E223.
15. Kadish AH, Little RL, Sternberg JC. A new and rapid method for the determination of glucose by measurement of rate of oxygen consumption. *Clin Chem* 1968;14:116–131.
16. Långström B, Antoni G, Gullberg P, et al. Syntesis of L- and D-[methyl-^{11}C]methionine. *J Nucl Med* 1987;28:1037–1040.
17. Någren K. Quality control aspects in the preparation of [^{11}C]methionine. In: Mazoyer BM, Heiss WD, Comar D, eds. *PET studies on amino acid metabolism and protein synthesis*. Dordrecht, Netherlands: Kluwer Academic Publishers; 1993:81–87.
18. Spinks TJ, Jones T, Gilardi MC, Heatrec JD. Physical performance of the latest generation of commercial positron scanner. *IEEE Trans Nucl Sci* 1988;35:721–725.
19. Lundqvist H, Stålnacke CG, Långström B, Jones B. Labeled metabolites in plasma after intravenous administration of [$^{11}CH_3$]-L-methionine. In: Greiz T, Ingvar DH, Widen L, eds. *The metabolism of the human brain studied with positron emission tomography*. New York, NY: Raven Press; 1985:233–240.
20. Patlak CS, Blasberg RG. Graphical evaluation of blood-to-brain transfer constants from multiple-time uptake data: generalizations. *J Cereb Blood Flow Metab* 1985;5: 584–590.
21. Sullivan JL, Debusk AG. Transport of L-methionine in human diploid fibroblast strain WI38. *Biochem Biophys Acta* 1978;508:389–400.
22. Lung MA. Variations in blood flow on mandibular glandular secretion to autonomic nervous stimulation in anaesthetized dogs. *J Phys Lond* 1990;431:479–493.
23. Martinoli C, Derchi LE, Solbiati L, Rizzato G, Silvestri E, Gianno M. Color doppler sonography of salivary glands. *Am J Roentgenol* 1994;163:933–941.
24. Ishiwata K, Kameyama M, Hatazawa J, Kubota K, Ido T. Measurement of L-[methyl-^{11}C]methionine in human plasma. *Appl Radiat Isot* 1991;42:77–79.
25. Någren K, Lehikoinen P, Leskinen S. Synthesis of [^{11}C]Me-AIB, α-[^{11}C]methyl-amino-isobutyric acid, for PET examination of the amino acid uptake system A. *J Lab Compd Radiopharm* 1995;37:156–157.
26. Schmall B, Conti PS, Kiesewetter DO, Alauddin MM. Synthesis of α-(N-^{11}C-methyl)-aminoisobutyric acid. *J Lab Compd Radiopharm* 1995;37:150–152.
27. Fugawa NK, Minaker KL, Young VR, Rowe JW. Insulin dose-dependent reductions in plasma amino acids in man. *Am J Physiol* 1986;250:E13–E17.
28. Castellino P, Luzi L, Simonson DC, Haymond M, DeFronzo RA. Effect of insulin and plasma amino acid concentrations on leucine metabolism in man. *J Clin Invest* 1987;80:1784–1793.
29. Stout DB, Huang SC, Raleigh MJ, Phelps ME, Melega WP. Concentration-dependent effects of plasma amino acid levels on 6[^{18}F]fluoro-L-DOPA uptake with PET [Abstract]. *J Nucl Med* 1996;37(suppl):109P.

Fluoride Kinetics of the Axial Skeleton Measured in Vivo with Fluorine-18-Fluoride PET

Christiaan Schiepers, Johan Nuyts, Guy Bormans, Jan Dequeker, Roger Bouillon, Luc Mortelmans, Alfons Verbruggen and Michel De Roo

Departments of Nuclear Medicine and Internal Medicine, University Hospital Gasthuisberg; and Laboratory of Radiopharmaceutical Chemistry, KU Leuven, Leuven, Belgium

The aim of this study was to quantify regional bone blood flow and influx rate with PET and [^{18}F]fluoride in patients with metabolic bone disorders. **Methods:** Dynamic imaging of the spine or pelvis was performed after administration of 300–370 MBq of $^{18}F^-$. Plasma clearance of $^{18}F^-$ was determined in blood sampled from the radial artery. A three-compartment model was used to estimate the regional flow and fluoride influx rate. **Results:** In this preliminary study, fluoride flux (in μmol/min/liter) could be measured regionally. The flux was consistent with the pathophysiology of the studied metabolic disorders and allowed the various disease states to be distinguished. Bone blood flow and influx rate were low in osteoporosis (in the "normal-appearing" bone) and high in Paget's disease. **Conclusion:** With PET and [^{18}F]fluoride, local bone blood flow and fluoride influx rate can be quantified in patients in vivo. Metabolically active zones have an increased influx rate and an accordingly increased flow. In principle, this technique permits classification of bone disorders and has potential for the monitoring of therapy response in metabolic bone disease.

Key Words: ^{18}F; skeletal flow; PET; metabolic bone disease

J Nucl Med 1997; 38:1970–1976

The usefulness of $^{18}F^-$ for skeletal imaging was demonstrated decades ago by Blau et al. (*1*), and it subsequently became the standard bone scan in clinical practice (*2*). The uptake of fluoride in bone is rapid and occurs primarily by chemisorption onto hydroxyapatite, followed later by exchange with hydroxyl groups in the hydroxyapatite. After intravenous administration, the radiopharmaceutical accumulates in the perivascular fluid, and the initial $^{18}F^-$ skeletal distribution is regarded as an indicator of blood flow to bone (*3*). In areas of high osteoblastic activity, immature bone is present, which has a large surface area to adsorb the radiopharmaceutical. Charkes et al. (*4,5*) emphasized the difference between skeletal flow and fluoride uptake and mathematically analyzed the contributions of the different compartments. Based on this compartmental model, they elegantly described the implications for routine skeletal scintigraphy in classifying normal and abnormal bone, both in general and in focal disease states (*6*). Using clearance techniques in animals, Wootton et al. (*7–9*) showed that the unidirectional extraction fraction of $^{18}F^-$ in bone was 1 and that the marrow uptake was negligible. Reeve et al. (*10*) found a significant correlation between initial fluoride uptake and Ca^{2+} influx. In addition, two histological indices correlated with the fluoride uptake, i.e., fraction of osteoid taking up double label and corrected apposition rate, revealing the correspondence between fluoride uptake and bone metabolic rate.

PET permits quantification of biochemical processes in vivo and is routinely used in neurological, cardiac and oncological applications (*11,12*). In a previous study from the University of California at Los Angeles (UCLA) (*13*), the application of

Received Nov. 12, 1996; revision accepted Mar. 19, 1997.

For correspondence or reprints contact: Christiaan Schiepers, MD, PhD, Department of Radiological Sciences, Olive View–UCLA Medical Center, 14445 Olive View Drive, Sylmar, CA 91342.

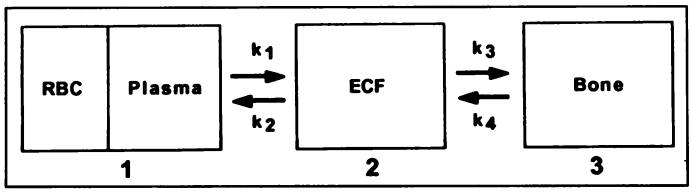

FIGURE 1. Fluoride kinetic model with three compartments: vascular (compartment 1), extracellular (compartment 2) and bone (compartment 3). RBC, red blood cells; ECF, extracellular fluid; k_1–k_4, diffusion rate constants. Arrows indicate the direction. Rate constants k_1 and k_2 represent forward and reverse transport from plasma, respectively, and k_3 and k_4 represent the uptake and release from bone, respectively. k_1 is equal to the local skeletal flow if the extraction fraction of the tracer equals 1. These rate constants are estimated with nonlinear regression.

[^{18}F]fluoride-PET with the whole-body imaging technique was reported for the workup of bone malignancies.

Here, we concentrated on the determination of the flow and influx rate of fluoride into the axial skeleton. The spine and pelvis were selected as the main areas of interest because these structures are relatively large and nonmoving in a resting supine patient. Regional bone blood flow and fluoride influx were estimated with compartmental modeling. Results for normal human vertebrae were reported previously by Schiepers et al. (*14*) and Hawkins et al. (*15*).

The relationship between $^{18}F^-$-PET kinetics and bone histomorphometry in renal osteodystrophy was investigated by Messa et al. (*16*). Recently, Berding et al. (*17*) reported a study in which the [^{18}F]fluoride-PET method was used to evaluate bone graft viability. Earlier, bone blood flow was studied in tibial fractures with PET in a semiquantitative way by Ashcroft et al. (*18*) using [^{15}O]H_2O. Bone marrow flow has been analyzed with PET using [^{15}O]carbon dioxide by Martiat et al. (*19*) in hematological disorders and using [^{15}O]H_2O by Kahn et al. (*20*) in normal volunteers.

Here, we investigated the bone blood flow, fluoride influx and flux in metabolic bone disease, specifically, of involved and "normal-appearing" areas. The quantitative results of the vertebrae were compared to those obtained previously in normal volunteers acquired with a similar PET system and acquisition protocol (*14,15*). Another aim of this preliminary study was to derive quantitative parameters for distinguishing disease states.

MATERIALS AND METHODS

Imaging was performed with a Siemens/CTI ECAT-931 system (Knoxville, TN). The patient's spine, pelvis or bone structure of interest was positioned in the scanner. A transmission scan was acquired to correct for attenuation effects of the tissues between the origin of photons and the detectors.

Fluorine-18-fluoride was produced by 10-MeV proton irradiation of 300 μl of [^{15}O]H_2O (Isotec, OH) in a Cyclone 10/5 cyclotron (IBA, Louvain-la-Neuve, Belgium). The irradiated [^{15}O]H_2O was passed over an anion exchange membrane (Bio-Rex AG1-X8, with a diameter of 4 mm; Bio-Rad, Richmond, CA). Fluorine-18-fluoride was eluted from the membrane with 3.5 mg of $KHCO_3$ dissolved in 700 μl of H_2O. The eluate was neutralized and passed over a sterile 0.22-μm filter.

A dose of 300–370 MBq of $^{18}F^-$ was injected in an antecubital vein as a bolus, and dynamic images were acquired for 1–2 hr over the thoracic or lumbar spine or pelvis. Fifteen transaxial planes were reconstructed with a thickness of 6.75 mm. Tracer plasma clearance was determined by sampling blood from the radial artery. Phantoms were used to calibrate the count rates between the PET scanner and the arterial blood counting device. Both whole-blood and plasma fluoride concentrations were analyzed.

By drawing regions of interest, we obtained time–activity curves of regional skeletal uptake. Mathematical modeling (Fig. 1) was applied to estimate the rate constants between the different compartments, i.e., vascular, perivascular and cellular spaces. This tracer kinetic model is the same as that used by Hawkins et al. (*15*) and differs from the whole-body kinetic model of Charkes et al. (*4,5*) in that it is regional, without the need for a renal or total-body compartment. Rate constants k_1 and k_2 represent forward and reverse transport from plasma, respectively, and k_3 and k_4 represent the uptake and release from bone, respectively. If f is the extraction fraction of the tracer, regional bone blood flow is represented by Equation 1:

$$\text{Flow} = f \times k_1 \quad (\text{in ml/min/ml}). \qquad \text{Eq. 1}$$

k_1 is equal to the local skeletal flow if the extraction fraction f equals 1, for which there exists experimental evidence (*7,9*). If the specific mass of bone involved (ρ, in g/ml) is known, the regional perfusion, i.e., concentration per mass tissue, can be calculated as:

$$\text{Perfusion} = f \times k_1/\rho \quad (\text{in ml/min/g}). \qquad \text{Eq. 2}$$

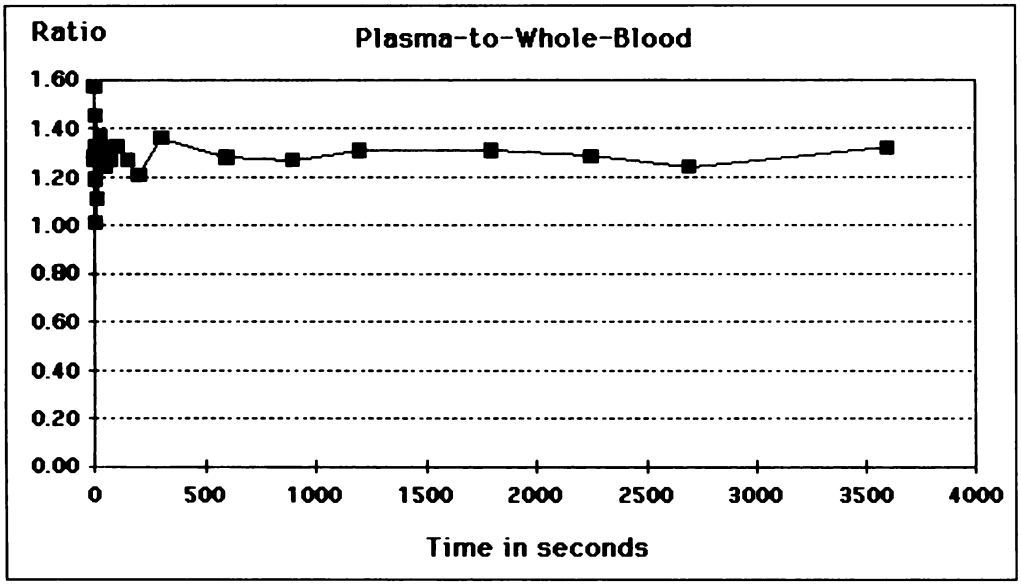

FIGURE 2. Ratio of the fluoride concentration in plasma to whole blood as a function of time. All values after the initial equilibration interval of 30 sec were entered. The total number of data points from all nine patients is 144. Note the larger scatter around the mean of 1.3 at the beginning of the study.

TABLE 1
Range of Blood Flow and Influx Rate in Normal-Appearing Bone of Osteoporosis Patients

Type of osteoporosis	n	Area	Flow (ml/min/ml)	Influx (K_i) (ml/min/ml)
Old age	4	Lumbar spine	0.06–0.09	0.035–0.049
		Ilium	0.03–0.08	0.019–0.036
		Sacrum	0.04–0.06	0.018–0.032
Juvenile	1	Thoracic spine	0.11–0.29	0.050–0.071

TABLE 2
Range of Bone Blood Flow and Influx Rate in Two Patients with Paget's Disease

	Abnormal bone regions		Contralateral control regions	
Area	Flow (ml/min/ml)	Influx (ml/min/ml)	Flow (ml/min/ml)	Influx (ml/min/ml)
Lumbar spine	0.19–0.24	0.139–0.160		
Pelvis	0.14–0.29	0.074–0.147	0.03–0.07	0.019–0.063

It is customary to express the perfusion per 100 g of tissue. Macro K is the net forward transport rate of fluoride to the bone compartment, i.e., fluoride influx rate, and is defined as:

$$K_i = k_1 \times k_3/(k_2 + k_3) \quad \text{(in ml/min/ml)}. \qquad \text{Eq. 3}$$

Here, k_1 and K_i are both expressed as rates per unit volume, i.e., ml/min per ml of tissue. When the plasma fluoride concentration ($[^{19}F^-]$, in μmol/liter) and the specific mass (ρ, in g/liter) are known, the net mass flux to bone equals:

$$\text{Mass flux} = \lambda \times K_i \times [^{19}F^-]/\rho \quad \text{(in μmol/min/g)}. \qquad \text{Eq. 4}$$

In Equation 4, λ is the lumped constant, indicating the difference in biological behavior between radioactive and stable tracer. For fluoride, $^{18}F^-$ and $^{19}F^-$ have the same chemical properties, and therefore λ = 1. Another way of expressing the flux is in units of concentration per volume:

$$\text{Volume flux} = \lambda \times K_i \times [^{19}F^-] \quad \text{(in μmol/min/liter)}. \qquad \text{Eq. 5}$$

Turnover half times of tracer in compartments 2 and 3 can also be calculated. The following equations hold for the model of Figure 1:

$$T_{1/2} \text{ (compartment 2)} = T_2 = 0.693/(k_2 + k_3) \quad \text{(in min)}. \qquad \text{Eq. 6}$$

and

$$T_{1/2} \text{ (compartment 3)} = T_3 = 0.693/k4 \quad \text{(in min)}. \qquad \text{Eq. 7}$$

The interpolated plasma clearance curve gave the tracer concentration in the vascular compartment as a function of time and served as the input function. An additional parameter, the so-called blood pool term (BV), was also estimated. BV represents the vascular blood in the studied tissue volume and is expressed as a percentage of the input function. Using iterative least squares fitting, the rate constants were adjusted to obtain optimal correspondence between the sum of the tracer concentrations in compartments 2 and 3 (extracellular and bone) and the time–activity curves in the regions of interest. The corresponding covariance matrix is not diagonal. This means that the estimates of the individual rate constants are not independent, and as a result, errors on one estimate propagate to the others. However, it can be shown that these errors partially cancel out in the computation of the macro K or influx rate. Consequently, the precision on the estimate of macro K is better than that on the individual rate constants. A more detailed description of the model and alternate approach to derive macro K with the Patlak graphical analysis is given by Hawkins et al. (*15*).

Fluoride concentration was determined with gas chromatography by the Pharmacy Laboratory at the University of Utrecht (Utrecht, Netherlands). The procedure is described by Glerum et al. (*21,22*) and yields the fluoride plasma concentration in μmol/liter. Special tubes that were low in CaF_2 were used to ensure the absence of fluoride cross-contamination.

We investigated nine patients with metabolic bone disorders: involutional osteoporosis (n = 4), Paget's disease (n = 2), primary hyperparathyroidism (n = 2) and juvenile osteoporosis (n = 1). All patients, with the exception of the patient with juvenile osteoporosis (age, 30 yr), were over 50 yr old (mean, 63 yr; range, 52–78 yr); there were five women and four men.

RESULTS

Fluoride Distribution

Fluorine-18-fluoride concentrations in both plasma and whole blood were counted. About 20 sec after the intravenous administration of the radiopharmaceutical, the count rate in the contralateral radial artery was sufficiently high for reliable count rate estimates, and the plasma-to-whole blood ratio had stabilized. For the detailed analysis, 30 sec after injection was arbitrarily selected as the starting point. All values thereafter were entered, yielding 144 sampling points for both plasma and whole blood in these nine patients. The average plasma-to-whole

TABLE 3
Average Data in Metabolic Bone Disease

Disorder	n	Age (yr)	Biochemistry Ca	PO_4	AF	F	BMD (%)	Flow (ml/min/ml) Mean	s.d.	Influx rate (ml/min/ml) Mean	s.d.	Flux (μmol/min/liter) Mean	s.d.
Osteoporosis*													
Old	4	63	8.9	5.2	162	24	68	0.058	0.020	0.022	0.014	0.023	0.010
Juvenile	1	30	8.9	3.1	220	15	59	0.200		0.059		0.047	
Paget's disease†	2	69	9.0	3.6	751	31	86	0.205	0.009	0.114	0.008	0.185	0.004
Hyperparathyroidism*	2	54	11.0	1.7	181	46	—	0.101	0.003	0.034	0.003	0.080	0.019
Normal men*‡	11	40	—	—	—	—	—	0.106	0.054	0.036	0.006	0.133	0.054§

*Vertebral bodies.
†Affected zones in the pelvis.
‡Volunteers from UCLA (*15*).
§Flux based on three normal subjects.
Ca = serum calcium in mg/dl; PO_4 = serum phosphate in mg/dl; AF = serum alkalic phosphatase in IU/liter; F = serum fluoride in μg/liter; BMD = bone mineral density of L2–L4 vertebrae determined with dual energy X-ray absorptiometry in percentage of age-matched controls.

TABLE 4
Individual Patient Data

Disorder	Age (yr)	Sex	Biochemistry Ca	PO_4	AF	F	BMD (%)	Three-compartment parameters k_1	k_2	k_3	k_4	BV	T_2	T_3	K_i	Flux (μmol/min/liter)
Osteoporosis*																
Old	63	M	7.9	4.4	96	24	68	0.077	0.225	0.179	0.012	0.006	2.4	105	0.041	0.037
								[0.012]	[0.160]	[0.095]	[0.009]	[0.012]	[1.6]	[92]	[0.005]	[0.015]
	78	F	10.2	7.2	108	26	67	0.048	0.369	0.107	0.004	0.007	2.7	180	0.012	0.016
								[0.019]	[0.310]	[0.063]	[0.002]	[0.010]	[2.3]	[92]	[0.004]	[0.055]
	68	F	8.5	4.1	58	26	80	0.035	0.105	0.059	0.003	0.005	5.6	187	0.012	0.016
								[0.011]	[0.057]	[0.027]	[0.002]	[0.006]	[3.9]	[42]	[0.003]	[0.038]
	52	F	9.1	4.5	385	19	58	0.072	0.225	0.170	0.000	0.030	1.8	741	0.024	0.024
								[0.016]	[0.075]	[0.023]	[0.001]	[0.028]	[0.4]	[155]	[0.006]	[0.057]
Juvenile	30	M	8.9	3.1	220	15	59	0.200	0.335	0.179	0.009	0.046	1.5	71	0.059	0.047
								[0.054]	[0.220]	[0.065]	[0.003]	[0.040]	[1.2]	[12]	[0.009]	[0.069]
Paget's disease†	69	F	9.5	3.8	942	32	81	0.198	0.304	0.334	0.002	0.011	1.5	273	0.108	0.182
								[0.057]	[0.230]	[0.170]	[0.002]	[0.005]	[0.8]	[123]	[0.025]	[0.041]
	68	M	8.5	3.3	560	30	90	0.211	0.199	0.323	0.008	0.003	1.4	155	0.119	0.188
								[0.021]	[0.051]	[0.065]	[0.002]	[0.002]	[0.3]	[60]	[0.017]	[0.028]
Hyperparathyroidism*	56	F	11.2	1.4	114	35	—	0.103	0.320	0.163	0.010	0.020	1.8	68	0.036	0.066
								[0.033]	[0.170]	[0.047]	[0.005]	[0.022]	[1.0]	[26]	[0.004]	[0.076]
	52	M	10.8	1.9	248	57	—	0.099	0.303	0.142	0.014	0.013	1.8	51	0.031	0.093
								[0.020]	[0.115]	[0.061]	[0.004]	[0.014]	[0.7]	[14]	[0.006]	[0.017]
Normal men*‡	40	M	—	—	—	—	—	0.106	0.258	0.132	0.002	0.079	4.3	3900	0.036	0.133§
								[0.054]	[0.160]	[0.030]	[0.001]	[0.065]	[2.1]	[6030]	[0.006]	[0.054]

*Vertebral bodies.
†Affected zones in the pelvis.
‡Volunteers from UCLA (11 male subjects) (*15*).
§Flux based on three normal subjects.
Values in brackets are s.d. k_1 and K_i are in ml/min/ml; k_2, k_3 and k_4 are in 1/min; and BV is in ml/ml.
M = male; F = female; Ca = serum calcium in mg/dl; PO_4 = serum phosphate in mg/dl; AF = serum alkalic phosphatase in IU/liter; F = serum fluoride in μg/liter; BMD = bone mineral density of L2–L4 vertebrae determined with dual energy x-ray absorptiometry in percentage of age-matched controls; T_2 and T_3 = turnover half times (in min) of tracer in compartments 2 and 3, respectively.

blood ratio was 1.30, with a s.d. of 0.09, and linear regression analysis of this ratio over time furnished a slope that did not differ significantly from 0. In Figure 2, the ratio of plasma to blood is plotted. Therefore, more of the injected tracer is available in the freely diffusable plasma compartment.

Inspection of the individual patient ratios did not reveal significant differences, indicating that there is no relationship between disease state and plasma/blood fluoride distribution.

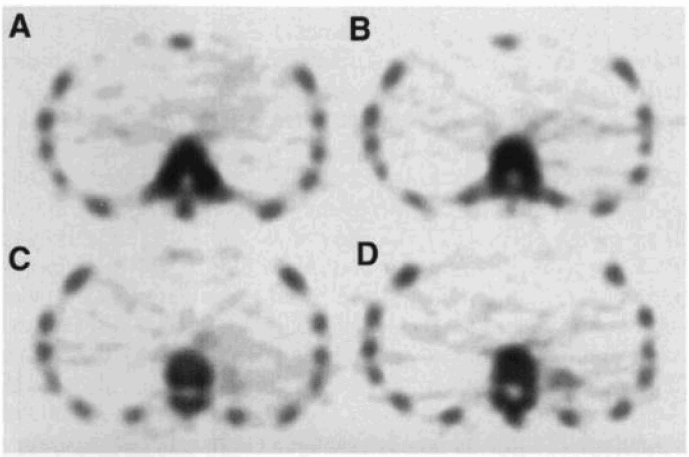

FIGURE 3. Transverse planes of the lumbar spine of a 52-yr-old woman with osteoporosis. The images were acquired between 45 min and 60 min after administration of 350 MBq of [^{18}F]fluoride. The gray levels from the image itself cannot be directly converted to skeletal flow or influx rate. Mathematical modeling is necessary to obtain these parameters. Note the detail of vertebral body, transverse and spinous processes. In the highest plane (A and B), degenerative changes are seen in the left facet joint.

Skeletal Flow and Flux

For the five osteoporosis patients, the range of flow and influx rate values is given in Table 1. Data are presented in ml/min/ml for certain areas of normal appearing bone. The difference between high-turnover osteoporosis in the 30-yr-old man and the other patients (mean age, 63 yr) is obvious.

Table 2 gives the bone blood flow and influx rate of the two patients with Paget's disease. In this disorder, we measured the highest flow and influx. Abnormal areas have a 3- to 5-fold increased flow and 2- to 3-fold increased influx rate compared to the contralateral control areas.

A summary of average values for the investigated metabolic

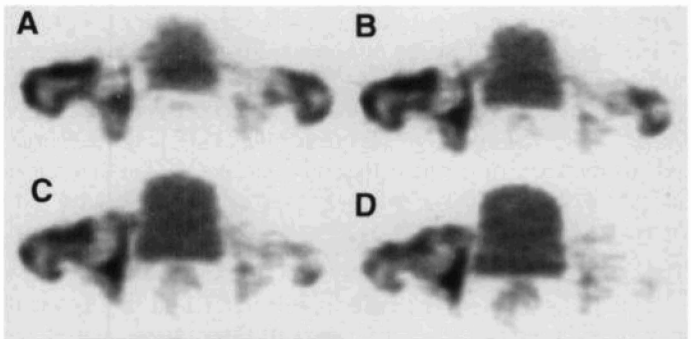

FIGURE 4. Paget's disease of bone in a 69-yr-old woman. Four consecutive transverse images at the level of the hips and lower sacrum (at the bottom of planes C and D). Note the high uptake in the affected bones in the right ischium and femoral head, whereas the not involved bones on the left are barely visible in this linear gray scale. The bladder is in the field of view and "hot" because fluoride is excreted in the urine (~25%).

FIGURE 5. A 77-yr-old woman with focally increased uptake in the thoracic spine. This coronal and sagittal plane of 81 cm in length reveals the compression fracture at T7. The whole-body images were acquired after the dynamic scan was completed. An additional unsuspected lesion was discovered in a vertebra two levels lower. Because the field of view of a PET scanner is limited, the area of interest for the PET study has to be defined beforehand with another imaging modality. In this patient, dynamic images of the lumbar spine were acquired; therefore, no dynamic images are available of the compression fracture to estimate flow and influx rate.

bone disorders is given in Table 3. As expected, osteoporosis in the elderly has both low flow and low influx rate, whereas juvenile osteoporosis and Paget's disease reveal the opposite pattern. Patients with hyperparathyroidism provided the same values as did the normal male volunteers from UCLA.

An overview of the individual patients is given in Table 4. Pertinent serum levels reveal the expected abnormalities for Paget's disease and primary hyperparathyroidism. The bone mineral density, expressed as a percentage of the age-matched controls, was most decreased in the osteoporotic patients. The flux, i.e., the net forward transport of fluoride from the vascular to bone compartment (Fig. 1), was calculated by using Equation 5. Calculation of the mass flux (Eq. 4) requires the regional specific mass. Table 4 shows a wide range of bone mineral density values, and both trabecular and cortical bone were investigated; therefore, the true regional specific mass will vary considerably per patient and must be measured independently.

As Table 4 suggests, the flux appeared to have the highest power to distinguish the disorders. However, determination of fluoride concentration is not a routine laboratory procedure. Therefore, flow and influx rates with dimensions of ml/min/ml are usually calculated with the [^{18}F]fluoride-PET method. Table 3 shows that the patients with involutional osteoporosis and Paget's disease have flow and influx rate values at the extremes, when compared to normal vertebral bodies of the thoracic spine, as reported previously by Hawkins et al. (*15*) (last rows of Tables 3 and 4).

Clinical Cases

Typical transverse slices of the lumbar vertebrae at the end of a dynamic scan are given in Figure 3. From these images, the skeletal flow and influx cannot be assessed visually.

In Figure 4, images of the hips and pelvis of the patient with long-standing Paget's disease are shown. Note the increased fluoride uptake in the involved right hip compared to the normal left hip.

In Figure 5, a representative coronal and sagittal plane of a whole-body PET is shown. The study was performed in a typical osteoporosis patient. Note the high fluoride uptake in the compression fractures. The whole-body images were acquired after completion of the dynamic scan and were acquired as a set of sequential volumetric images.

DISCUSSION

With $^{18}F^-$-PET, we were able to obtain estimates of regional skeletal blood flow in vivo. To our knowledge, Nahmias et al. (*23*) published the first paper on skeletal flow determination with [^{18}F]fluoride and a modern-type PET scanner in dogs. However, they did not supply a direct correlation of the PET results with invasive flow methods, such as microspheres. The quantitative [^{18}F]fluoride PET method was later applied to humans by the UCLA group (*13–16*). Here, we have shown that the procedure may be applied to patients who tolerated the sometimes lengthy imaging times well.

The plasma-to-blood ratio appeared constant after an initial 0.5 min of equilibration time (Fig. 2). We did not find a decreasing ratio with time, as was reported by Hawkins et al. (*15*). This is likely related to the difference in the way the input function is acquired. We used true arterial sampling, whereas in the Hawkins' study, arterialized venous blood sampling was switched to normal venous sampling after 30 min. Figure 2 indicates that arterial blood instead of plasma can be used to measure the input function. Because the plasma-to-blood ratio is disorder-independent, an image-derived blood pool input function might be used as well, which greatly simplifies the procedure. The relationship of input functions (plasma, whole blood and left ventricular blood pool) and its effects on modeling of skeletal fluoride kinetics was reported earlier by us in the beagle dog (*24,25*).

Flow and influx were determined in three metabolic bone disorders. We found both a high flow and high influx rate for Paget's disease as expected (Tables 2–4). The opposite was demonstrated for osteoporosis in the elderly. Previously, we have described skeletal fluoride kinetics in normal male volunteers measured with PET and $^{18}F^-$ and found fluoride uptake to be a first-order process with a three-compartment model being the preferred kinetic structure (*14,15*). In this preliminary study, we have shown that the model also holds for pathological bone.

Given the relatively short half-life of ^{18}F (about 110 min) and PET acquisition times, reliable estimates of regional skeletal blood flow are possible. T_2 values are on the order of a few minutes (Eq. 6 and Table 4), and there is a trend of shorter half-times for the high-turnover metabolic disorders. On the other hand, T_3 values (Eq. 7) are much higher than T_2 values, by about 2 orders of magnitude (see Table 4), and a value of 65 hr has been reported for transport of fluoride into the normal bone compartment (*15*). Therefore, the fluoride clearance rate of bone mineral is probably too slow to be estimated reliably with PET, even for pathological bone with high turnover. Interestingly, the clearance half-time of the bone compartment (T_3) was similar for involutional osteoporosis and Paget's disease and was about the same as normal. On the contrary, in juvenile osteoporosis and hyperparathyroidism, T_3 appears decreased, suggesting increased turnover. The other kinetic parameters in hyperparathyroidism are the same as those in normal male volunteers. The fraction of tracer in the second compartment that will be transported to the bone compartment is $k_3/(k_2 + k_3)$, which is equal to the ratio K_i/k_1 and is about 1/3 for normal vertebra, hyperparathyroidism and both juvenile and involutional osteoporosis and about 1/2 for Paget's disease (Table 3). This latter finding with maintained turnover (T_3) suggests

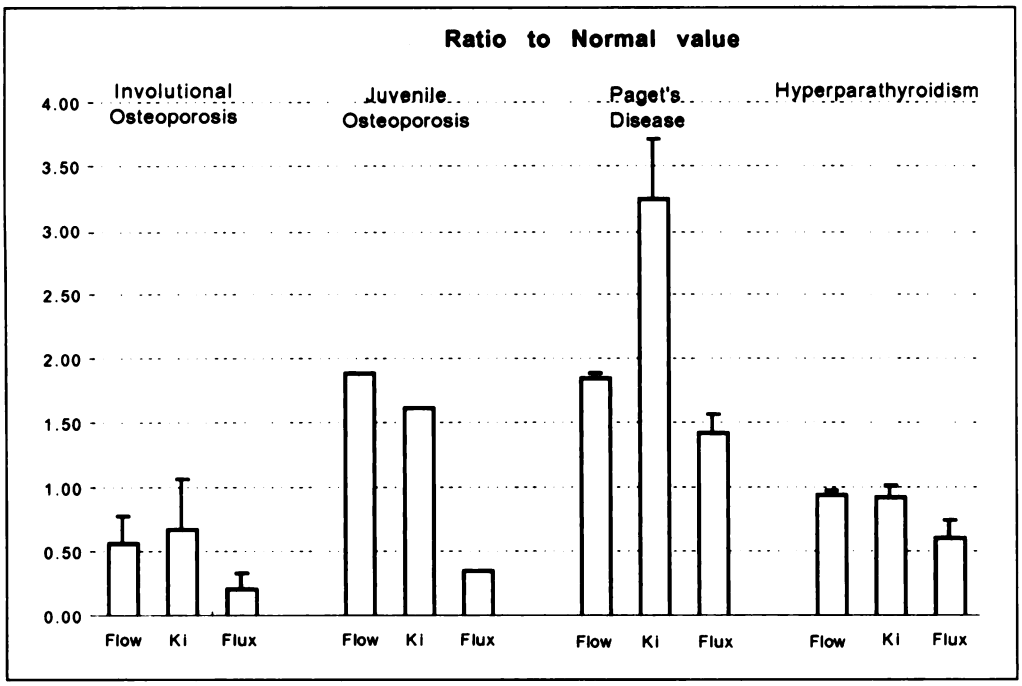

FIGURE 6. Comparison of our data in metabolic disorders to those of normal male subjects from Hawkins et al. (*15*). Columns represent mean pathological-to-normal ratios, and bars indicate 1 s.d.. Normal flow and influx rates (K_i) are based on 11 subjects, whereas the normal flux contains the average of 3 subjects (see Tables 3 and 4). The numbers of patients in the studied groups are: involutional osteoporosis, n = 4; juvenile osteoporosis, n = 1; Paget's disease, n = 2; and hyperparathyroidism, n = 2.

primary increased flow in Paget's disease. Juvenile osteoporosis, on the other hand, has a maintained K_i/k_1 ratio with increased turnover reflecting a secondarily increased flow. The K_i/k_1 ratio will remain unchanged if both k_2 and k_3 increase appropriately. PET is unique in permitting this type of regional analysis in vivo and will contribute significantly in understanding disease processes in bone at the physiologic and biochemical level.

Possible variations in regional extraction fraction might lead to underestimation of the flow (Eq. 1). However, this technique will still be able to estimate the distribution of skeletal flow, i.e., over the different regions and organs, with a much higher degree of accuracy than do whole-body clearance techniques. Conventional bone scintigraphy with ^{99m}Tc-labeled diphosphonates will also supply a map of the regional flow distribution. However, PET with [^{18}F]fluoride has the capability of absolute quantification of regional flow and flux.

If the specific mass of the tissue involved is known, multiplication with the regional flow (Eq. 2) yields the local perfusion in ml/min/g. The regional specific mass can be measured with quantitative CT, which is not a routine procedure. Mass flux can be determined if both specific mass and plasma fluoride concentration are known (Eq. 3). We evaluated the fluoride flux (expressed per volume; Eq. 4) and compared similar bone structures. The flux can be used to separate high from low "bone-turnover" states (Table 4). Hawkins et al. (*15*) supplied plasma fluoride levels around 3 μmol/liter in three volunteers. For our patients, we found an average serum level of 29 μg/liter, corresponding to 1.4 ± 0.8 μmol/liter (Tables 3 and 4), which is within the normal range for Northern Europe (*17,21,22*). A direct comparison between pathological and normal bone was attempted by calculating the ratios for the flow, influx rate and flux. The results are given in Figure 6 and reveal the discriminating power of the flux. Both involutional and juvenile osteoporosis had a decreased flux, whereas Paget's disease had increased values, and hyperparathyroidism showed values within the normal range. When influx rate K_i was used instead of fluoride flux, the values show a larger overlap, i.e., ratios of 1.6 in juvenile osteoporosis, 0.7 in involutional osteoporosis and 0.9 in hyperparathyroidism. In other words, the flux may be used for classification of metabolic bone disease and might also be useful for monitoring therapeutic interventions (*26*). Needless to say that the aforementioned observations are based on a limited number of patients and normal subjects. However, the use of PET and its quantitative aspects are elegantly disclosed in studying biological processes in vivo.

Quantitative estimates of k_1 (Table 4) in normal vertebrae by Hawkins et al. (*15*) correspond favorably to animal data with a perfusion of 5 ml/min/100 g in cortical and 16 ml/min/100 g in trabecular bone (*27–29*). We found 0.11 ml/min/ml in normal volunteers, which may be converted to 7.6 ml/min/100 g by using a specific mass for vertebrae of 1.4 g/ml (*14,15*). Pathological bone showed the expected trend depending on the disorder: osteoporosis showed low flow (Table 1 and Figs. 3, 5 and 6), and Paget's disease showed high flow (Table 2 and Figs. 4 and 6).

Wootton (*30*) has reviewed the measurement of normal bone blood flow in humans. In this excellent contribution, he compared the results of whole-body clearance techniques with ^{85}Sr or ^{18}F to the ^{133}Xe washout technique (*31*) and the PET method of Hawkins et al. (*15*). Remarkably, the results were quite similar, given the type of bone studied (cortical, trabecular or mixed), except for the data of Charkes et al. (*4–6*), which showed a clear-cut 2–3 times higher value than did the other studies. In general, the whole-body clearance methods provided a lower limit of skeletal perfusion that is inherent to the technique, whereas the regional methods yielded somewhat higher numbers. In an attempt to arrive at a consensus, Wootton (*30*) concluded that the estimated mean value of skeletal blood flow was 4% of cardiac output (range, 3.5%–9%), corresponding to a blood flow of 270 ml/min or skeletal perfusion of 3.4 ml/min/100 g for the standard man. However, an independent noninvasive determination of k_1 in humans is not possible. For vertebrae with abundance of trabecular bone, a higher value has to be expected. Thus, a close correspondence was observed between perfusion of normal vertebrae (*15*), our results for hyperparathyroidism (Table 4) and published animal data obtained with invasive techniques (*27–29*).

Wootton et al. (*32*) assessed skeletal flow in Paget's disease and found a wide range, from 1 to 5 times normal flow. Here, we found flow values in affected spine and pelvis to be twice as

high as values in the normal UCLA volunteers and three times those of the elderly with osteoporosis (Table 3). Comparison of values within the same patient with Paget's disease gave a flow of 0.089 ml/min/ml in the female patient and 0.054 in the male patient, yielding flow ratios of affected-to-normal bone of 2.2 and 3.9, respectively (see Tables 2 and 4). The same group [Green et al. (*33*)] reported that the skeletal blood flow in metabolic bone disorders showed a wide range with the largest variations in Paget's disease. Similar fluctuations occur in hematological disorders (*31*).

Based on the results of this investigation, the fluoride flux to the bone compartment is the parameter of choice to distinguish the metabolic bone disorders (Table 4 and Fig. 6). Because the fluoride concentration is not easy to determine and is only available in specialized laboratories, the influx rate K_i may be used instead. Thus, influx rate is high in bone disorders with increased metabolic turnover and low in (low-turnover) osteoporosis, i.e., in the normal appearing areas without fractures.

A drawback of this technology for routine skeletal fluoride measurements is the limited availability of PET and radioactive fluoride. However, the half-life of $^{18}F^-$ permits remote production of the radionuclide and transport of the tracer to satellite nuclear medicine departments. Another limitation is the axial field of view of current PET cameras, which is about 10–25 cm. Because dynamic imaging is necessary over a 1–2 hr period, only one specific body area can be studied during a single session. True whole-body PET with measurement of bone blood flow and flux in real time is not yet feasible.

The results of the present investigation and the observed trends need to be corroborated in larger series. Also, the application of this tool in clinical practice needs to be addressed, and further research is indicated to establish the proper indications for quantification of flow and flux in bone disorders.

CONCLUSION

Regional flow and influx rate, as well as flux, can be determined in vivo with PET. Flow and influx vary, depending on the type of bone, turnover rate and presence of metabolic disease. Abnormal bone showed different flow and influx rates compared to normal areas. Paget's disease had the highest flow and influx rates, whereas involutional osteoporosis had the lowest values. In principle, it is possible to characterize the severity of metabolic bone disorders with [^{18}F]fluoride PET. The application of this method, allowing for an instantaneous measurement of flow and influx rates, may have potential utility in assessing the severity of a patient's disease or in monitoring the effect of treatment. The possible indications in clinical routine need further investigation.

ACKNOWLEDGMENTS

This study was supported by Belgian National Fund for Scientific Research Grant 3.0116.91 (Brussels, Belgium). We are indebted to Sung-Cheng Huang, PhD, for his help with revising the modeling aspects of the manuscript, and our stimulating discussions with him were greatly appreciated.

REFERENCES

1. Blau M, Nagler W, Bender MA. Fluorine-18: a new isotope for bone scanning. *J Nucl Med* 1962;3:332–334.
2. Blau M, Ganatra R, Bender MA. ^{18}F-Fluoride for bone imaging. *Semin Nucl Med* 1972;2:31–37.
3. Van Dyke D, Anger HO, Yano Y, Bozzini C. Bone blood flow shown with ^{18}F and the positron camera. *Am J Physiol* 1965;209:65–70.
4. Charkes ND, Makler PT, Philips C. Studies of skeletal tracer kinetics: I. Digital-computer solution of a five-compartment model of [^{18}F]fluoride kinetics in humans. *J Nucl Med* 1978;19:1301–1309.
5. Charkes ND, Brookes M, Makler PT. Studies of skeletal tracer kinetics: II. Evaluation of a five-compartment model of [^{18}F]fluoride kinetics in rats. *J Nucl Med* 1979;20: 1150–1157.
6. Charkes ND. Skeletal blood flow: implications for bone scan interpretation. *J Nucl Med* 1980;21:91–98.
7. Wootton R. The single-passage extraction of ^{18}F in rabbit bone. *Clin Sci Mol Med* 1974;47:73–77.
8. Wootton R, Reeve J, Veall N. The clinical measurement of skeletal blood flow. *Clin Sci Mol Med* 1976;50:261–268.
9. Wootton R, Dore C. The single-passage extraction of ^{18}F in rabbit bone. *Clin Phys Physiol Meas* 1986;7:333–343.
10. Reeve J, Arlot M, Wootton R, et al. Skeletal blood flow, iliac histomorphometry, and strontium kinetics in osteoporosis: a relationship between blood flow and corrected apposition rate. *J Clin Endocrinol Metab* 1988;66:1124–1131.
11. Phelps ME, Mazziotta JC, Schelbert HR, Eds. *Positron emission tomography and autoradiography: principal applications for the brain and the heart.* New York: Raven Press, 1986:493–661.
12. Schiepers CWJ. Whole body imaging with positron emission tomography: application in staging of malignancies. *Intern Med* 1994;2:17–23.
13. Hoh CK, Hawkins RA, Dahlbom M, et al. Whole body skeletal imaging with [^{18}F]-fluoride ion and PET. *J Comput Assisted Tomogr* 1993;17:34–41.
14. Schiepers CWJ, Hawkins RA, Choi Y, et al. Kinetics of bone metabolism assessed with $^{18}F^-$ and PET. *Eur J Nucl Med* 1990;16:450.
15. Hawkins RA, Choi Y, Huang SC, et al. Evaluation of the skeletal kinetics of ^{18}F-fluoride ion with PET. *J Nucl Med* 1992;33:633–642.
16. Messa C, Hoh CK, Choi Y, et al. Bone metabolic activity measured with PET and [^{18}F]-fluoride ion in renal osteodystrophy: correlation with bone histomorphometry. *J Clin Endocrinol Metab* 1993;77:949–955.
17. Berding G, Burchert W, van den Hoff J, et al. Evaluation of the incorporation of bone grafts used in maxillofacial surgery with [^{18}F]fluoride ion and dynamic positron emission tomography. *Eur J Nucl Med* 1995;22:1133–1140.
18. Ashcroft GP, Evans NT, Roeda D, et al. Measurement of blood flow in tibial fracture patients using positron emission tomography. *J Bone Jt Surg Br.* 1992;74:673–677.
19. Martiat Ph, Ferrant A, Cogneau M, et al. Assessment of bone marrow blood flow using positron emission tomography: no relationship with bone marrow cellularity. *Br J Haematol* 1987;66:307–310.
20. Kahn D, Weiner J, Ben-Haim S, et al. Positron emission tomographic measurements of bone marrow blood flow to the pelvis and lumbar vertebrae in young normal adults. *Blood* 1994;83:958–963.
21. Glerum JH, Van Dijk A, Klein SW, Nuyen WC. A general system for the automation of a backflush equipped gas chromatograph and its application in the determination of fluoride in plasma and feces. *Pharm Week Sci Ed* 1985;7:117–120.
22. Glerum JH. Fluoride in osteoporosis [doctoral thesis]. Utrecht, The Netherlands: University of Utrecht, 1987.
23. Nahmias C, Cockshott WP, Belbeck LW, Garnett ES. Measurement of absolute bone blood flow by positron emission tomography. *Skel Radiol* 1986;15:198–200.
24. Schiepers C, Vleugels S, Poppe G, et al. Estimation of bone blood flow and influx rate with $^{18}F^-$ and PET. *J Nucl Med* 1992;33:937.
25. Schiepers C, Geusens P, Yiang J, et al. Skeletal fluoride kinetics with PET and bone mineral density with DXA in beagles with nutritional osteoporosis. *J Nucl Med* 1993;34:141P.
26. Schiepers C, Geusens P, Vleugels S, et al. Positron emission tomography (PET) with $^{18}F^-$ to evaluate metabolic rate in bone disorders. *J Miner Bone Res* 1991;6(suppl): S243.
27. Morris MA, Kelly PJ. Use of tracer microspheres to measure bone blood flow in conscious dogs. *Calcif Tissue Int* 1980;32:69–76.
28. Simonet WT, Bronk JT, Pinto MT, et al. Cortical and cancellous bone: age related changes in morphological features, fluid spaces and calcium homeostasis in dogs. *Mayo Clin Proc* 1988;63:154–160.
29. Li G, Bronk JT, Kelly PJ. Canine blood flow estimated with microspheres. *J Orthop Res* 1989;7:61–67.
30. Wootton R. Measurement of bone blood flow in humans. In: Schoutens A, Arlet J, Gardeniers J, Hughes S, eds. *Bone circulation and vascularization in normal and pathological conditions*, pp 85–94. New York: Plenum Press, 1993.
31. Lahtinen R, Lahtinen T, Ramppanen T. Bone and bone marrow blood flow in chronic granulocytic leukemia and primary myelofibrosis. *J Nucl Med* 1982;23:218–224.
32. Wootton R, Tellez M, Green JR, Reeve J. Skeletal blood flow in Paget's disease of bone. *Metab Bone Dis Relat Res* 1981;4-5:263–270.
33. Green JR, Reeve M, Tellez N, et al. Skeletal blood flow in metabolic disorders of the skeleton. *Bone* 1987;8:293–297.